04,06

# Structure and electrical properties of Na-modificated spinel $LiNi_{0.5}Mn_{1.5}O_4$

© D.V. Lymar[1], E.V. Glazunova[1,2,¶], L.A. Shilkina[1], E.S. Kulikova[3], A.V. Nazarenko[4], A.A. Spivakov[1], I.A. Verbenko[1], S.V. Khasbulatov[2], L.A. Reznichenko[1]

[1] Institute of Physics, Southern Federal University, Rostov-on-Don, Russia
[2] Kh. Ibragimov Complex Institute of the Russian Academy of Sciences, Groznyi, Russia
[3] National Research Center „Kurchatov Institute", Moscow, Russia
[4] Southern Scientific Center, Russian Academy of Sciences, Rostov-on-Don, Russia
[¶] E-mail: glazunova@sfedu.ru

*Received July 18, 2025*
*Revised October 22, 2025*
*Accepted October 25, 2025*

The paper presents the results of X-ray diffraction analysis, microstructure and dielectric characteristics studies of solid solutions in the $Li_{1-x}Na_xNi_{0.5}Mn_{1.5}O_4$ system. X-ray diffraction analysis showed that solid solutions in the $Li_{1-x}Na_xNi_{0.5}Mn_{1.5}O_4$ system have a disordered structure of the Fd3m spinel type. The introduction of $Na^+$ into the system leads to the formation of NiO and $LiMnO_2$ impurity phases, the concentration of which increases with increasing $Na^+$ concentration. It is shown that the introduction of $Na^+$ into the system leads to a decrease in the cell parameter, which indicates its non-inclusion or limited inclusion in the $LiNi_{0.5}Mn_{1.5}O_4$ crystal lattice. Analysis of the dielectric spectral dependencies showed that there is no transition to the ferroelectric phase in $Li_{1-x}Na_xNi_{0.5}Mn_{1.5}O_4$ solid solutions. The increase in electrical conductivity above 150 K is due to hopping conductivity.

**Keywords:** solid-phase synthesis, spinel-type structure, $LiNi_{0.5}Mn_{1.5}O_4$, modification, dielectric spectroscopy.

DOI: 10.61011/PSS.2025.10.62630.204-25

## 1. Introduction

Multiferroics, which simultaneously exhibit ferroelectric and ferromagnetic ordering, are currently of great interest to the researchers [1–2]. For commercial applications, it is important to achieve a strong interaction between ferroelectric polarization and magnetism to ensure mutual control of magnetic spins and electric dipoles by applying small external effects (voltage or magnetic field) with low energy losses, especially at room temperature [3–5]. Thus, understanding the basic mechanism of ferroelectricity and magnetism interaction is a key factor in designing the new multiferroics that may be used in magnetoelectric devices.

One of the promising classes of multiferroics are chemical compounds with a spinel-type structure with a wide range of magnetic and electrical properties [6–9]. Due to variety of magnetic properties and types of emerging magnetic orders in spinel, this class of materials looks promising for the search of multiferroics. The spinel structure can accommodate transition metals, which in many cases leads to different types of magnetic ordering at high temperatures. Despite the diversity of magnetic spinels, a relatively small number of multiferroic or magnetoelectric materials have been discovered among them so far [10]. A magnetoelectric coupling may arise only when the inversion center of the crystal structure is suppressed. In spinels, the presence of different types of atoms in cationic sub-lattices leads to potential atomic ordering, which can suppress the inversion center. However, in contrast to perovskite ferroelectric materials, no any intrinsic ferroelectricity was observed in spinels during the experiments, except for a suggestion on the non-centered position of B-cation along the crystallographic direction $\langle 111 \rangle$ [11] and on the relaxor ferroelectricity in $CdCr_2S_4$ spinel [12]. On the other hand, the diverse magnetic properties of spinels make them potentially promising for observing new effects in magnetoelectric and multiferroic compounds.

For example, $LiFe_5O_8$ can exist in a disordered form with a random distribution of cations, as well as in an ordered form that can be achieved by annealing at suitable temperatures. $LiFe_5O_8$ is featuring magnetic order at very high temperature ($T_c = 905$ K), however, the exact magnetic structure is still unknown [13]. The ordered structure of $LiFe_5O_8$ can be described by the spatial groups $P4_132$ or $P4_332$ (i.e. magnetoelectric interactions like $PM^2$ are prohibited). Despite this, the magnetoelectric effect has recently been confirmed in this spinel below room temperature [14], which can be explained by the

fact that higher-order magnetoelectric coupling ($PM^4$) is possible in it. Other spinels, e. g., $Mn^{4+}$ — containing $AM_{0.5}Mn_{1.5}O_4$ (A = Li, Cu; M = Ni, Mg), which exhibit ferro- or ferrimagnetism, are also possible in the cation-ordered structure of $P4_332$ and may demonstrate magnetoelectric properties [15], similar to $LiFe_5O_8$. E. g., the spinel $LiNi_{0.5}Mn_{1.5}O_4$ is itself a normal spinel where $Ni^{2+}$ and $Mn^{4+}$ are in the octahedral positions, and $Li^+$ are in the tetrahedral positions, i. e. $Li^+$ serves as A-cation, and $Ni^{2+}$ and $Mn^{4+}$ serve as B-cation. Depending on the location of cations $Ni^{2+}$ and $Mn^{4+}$ the spinel may have an ordered structure ($P4_332$) and disordered structure (Fd3m). For ordered spinel, small superstructural reflections of (110) and (320) are observed; in case of disordered spinel, these reflections are absent [16].

$LiNi_{0.5}Mn_{1.5}O_4$ are generally considered in publications for the purpose of electrochemical applications. The materials based on $LiNi_{0.5}Mn_{1.5}O_4$ spinel are reported to properly retain high voltage during charging/discharging at about 4.7 V. It is a promising cathode material for a new generation of high-voltage lithium-ion batteries [17]. It is also reported that doping of $LiNi_{0.5}Mn_{1.5}O_4$ with $Na^+$ cations affects both the size of crystal domains and the parameters of the crystal lattice, without changing the basic structure of spinel. Doping with $Na^+$ not only increases the disorder in the distribution of nickel and manganese cations in the spinel structure, but also adds two additional electron jump paths that improve charge transfer, reduce ohmic and electrochemical polarization of materials, and improve the diffusion coefficient of lithium ions [18].

$LiNi_{0.5}Mn_{1.5}O_4$ also exhibits ferrimagnetic ordering under temperatures below $T_N = 129$ K [19]. In this case, the magnetic order is itself a collinear ferrimagnetic order where both the Ni and Mn sub-lattices are ferromagnetic and spin-polarized in the opposite direction. The ferromagnetism of the Ni sublattice is due to its antiferromagnetic coupling with Mn sublattice, while the interactions of Ni−Ni are insignificant [20].

Despite the data available in the literature on the structure and electrochemical properties of $LiNi_{0.5}Mn_{1.5}O_4$, the dielectric and magnetic properties of these materials have been poorly studied.

In connection with the above, the purpose of this study is to find out the formation patterns for the phase composition, structure, and dielectric characteristics of solid solutions based on $LiNi_{0.5}Mn_{1.5}O_4$ modified with $Na^+$.

## 2. Objects and methods of research

The objects of research included solid solutions of $Li_{1-x}Na_xNi_{0.5}Mn_{1.5}O_4$, with $0.00 \le x \le 0.20$, $\Delta x = 0.05$. The following precursors, previously verified by X-ray phase analysis, were used as initial components for the synthesis of solid solutions: $NaHCO_3$ (c.p.), NiO (p.), $Mn_2O_3$ (e.p.) and $Li_2CO_3$ (c.p.).

The specimens were fabricated by two-stage solid-phase synthesis at $1170\,\text{K} \le T_{\text{synt}\,1} \le 1220\,\text{K}$ (during 5 h), and $1220\,\text{K} \le T_{\text{synt}\,2} \le 1270\,\text{K}$. Sintering was carried out using conventional ceramic technology at $1270\,\text{K} \le T_{\text{sint}} \le 1320\,\text{K}$ depending on the composition for 2 h.

Phase composition of specimens was studied using X-ray diffraction analysis (XRD) at Kurchatov Synchrotron Radiation Source [21] equipped with Rayonix SX165 two-dimensional CCD detector ($\lambda = 0.75$ Å, Si monochromator). The measurements were carried out at room temperature using transmission geometry method, the detector was located at a distance of 150 mm from the specimen at a deflection angle of 29.5° from the axis of the forward beam to maximize the angular scale. Shooting time for one image was 5 min. The diffraction patterns were converted to one-dimensional form $I(2\theta)$ using azimuth integration in Dionis program [22], the broadening of the diffraction lines was taken into account by measuring as per certified standard $LaB_6$ (NIST SRM 660a).

The content of the impurity phases was evaluated by a relative intensity of their strongest line: $I/I_1 \cdot 100\,\%$, where $I$ — intensity of the strong line of the impurity phase, $I_1$ — intensity of the strong line of the main phase.

The experimental ($\rho_{\text{exp}}$) specimens density was determined by hydrostatic weighing in *n*-octane.

The X-ray density ($\rho_{\text{XR}}$) was calculated using the formula:

$$\rho_{\text{XR}} = Z\frac{M}{N_A}V, \tag{1}$$

where $Z$ — number of formula units, $M$ — molecular mass per one formula unit, $N_A$ — is Avogadro's number, $V$ — lattice cell volume.

Relative density ($\rho_{\text{rel}}$) was found as follows:

$$\rho_{\text{rel}} = (\rho_{\text{exp}}/\rho_{XR}) \cdot 100\,\%. \tag{2}$$

The accuracy of the lattice cell parameters determination was found as: $\Delta a = \pm(0.002-0.004)$ Å.

The microstructure of the transverse ceramic cleavage was studied using a 3D color laser scanning microscope KEYENCE VK-9700 (in CRC „Joint Center for Scientific and Technological Equipment of Southern Scientific Center of the Russian Academy of Science (research, development, testing)“ (No. 501994)).

The dielectric measurements were carried out using a test bench equipped with Wayne Kerr 6500B impedance analyzer (in the temperature range 10−325 K). Frequency of the measurement electrical field varied from 100 Hz to 1 MHz. The specimens were cooled in a closed loop helium refrigerator CCS-150.

## 3. Experimental Results

Analysis of solid solutions diffraction patterns $Li_{1-x}Na_xNi_{0.5}Mn_{1.5}O_4$, obtained at sintering temperature of

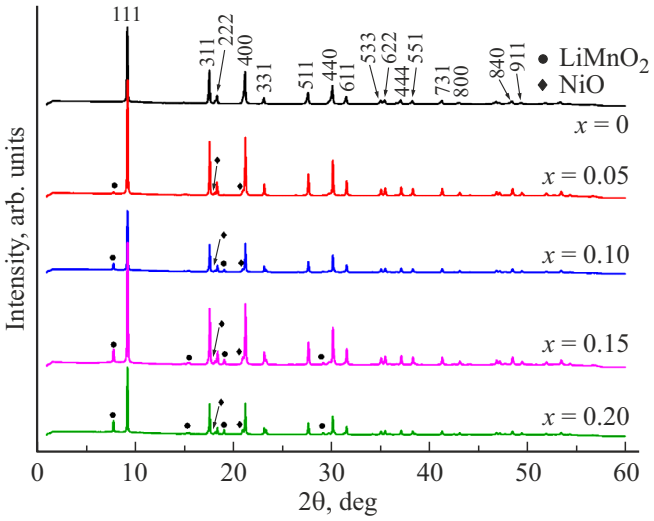


**Figure 1.** Diffraction patterns of the solid solutions system $Li_{1-x}Na_xNi_{0.5}Mn_{1.5}O_4$.

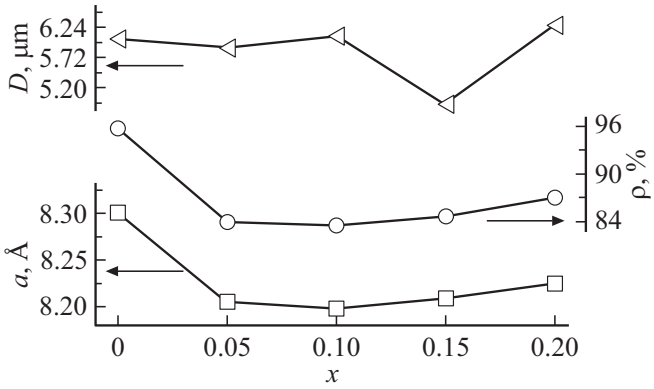


**Figure 2.** Dependencies of the lattice cell parameters, $a$, relative densities, $\rho_{rel}$, average grain sizes, $\overline{D}$ of the solid solutions system $Li_{1-x}Na_xNi_{0.5}Mn_{1.5}O_4$ versus concentration $x$.

1273 K, showed that pure $LiNi_{0.5}Mn_{1.5}O_4$ has no impurities (Figure 1). $Li_{1-x}Na_xNi_{0.5}Mn_{1.5}O_4$ can be characterized using spinel cubic structure with a spatial group Fd3m.

When 5 mol.% of $Na^+$ is introduced there remains some amount of NiO that didn't participate in the reaction. With the increase of $Na^+$ concentration of up to 10 mol.% apart from NiO [23] an impurity phase of $LiMnO_2$ also is formed [24]. With a further increase in the concentration of $Na^+$, the proportion of impurity phases rises. According to the diffraction patterns, the solid solution structure is disordered, as evidenced by the absence of diffraction reflections corresponding to the ordering [16]. The change in parameters of lattice cell, $a$, relative densities, $\rho_{rel}$, and average size of grains, $\overline{D}$ in the solid solutions of $Li_{1-x}Na_xNi_{0.5}Mn_{1.5}O_4$ system versus concentration $x$ are shown in Figure 2.

When $Na^+$ cations are introduced into the system, the cell parameter is diminished. This may indicate

Lattice parameters ($a$) for all specimens after sintering and ratios of/integral intensities $I(400)/I(311)$

| $x$ | $a$ (Å) | $I(400)/I(311)$ |
|---|---|---|
| 0.00 | 8.301 | 0.98 |
| 0.05 | 8.205 | 0.97 |
| 0.10 | 8.198 | 0.99 |
| 0.15 | 8.210 | 1.01 |
| 0.20 | 8.225 | 1.00 |

that $Na^+$ is practically not integrated into the structure of $LiNi_{0.5}Mn_{1.5}O_4$, since the ionic radius $Na^+$ is larger than $Li^+$ ($R(Na^+) = 0.98$ and $R(Li^+) = 0.68$) [25]. The decrease in the cell parameter may be due to the withdrawal of part of the B-cations from the structure, forming the impurity phases NiO and $LiMnO_2$. The degree of substituting ions filling in lithium positions 8$a$ can be represented by integral ratios of peak intensities (400)/(311) [19,26]. The ratio of peaks (400)/(311) for the obtained $LiNi_{0.5}Mn_{1.5}O_4$ remains practically unchanged when $Na^+$ is introduced into the system (table), which is also an evidence that $Na^+$ cannot be integrated into the lattice of $LiNi_{0.5}Mn_{1.5}O_4$.

Analysis of photographs of the microstructure of the solid solutions of system (Figure 3, $a$) showed that the average grain size varies from 4.9 to 6.3 $\mu$m (Figure 2) depending on the value of $x$. In all solid solutions the grains have a shape of polyhedrons.

When the concentration of $Na^+$ increases above 10 mol.%, needle-shaped grains appear (highlighted in Figure 3 with a dashed line), which is typical for the phase $LiMnO_2$ [27]. At $x = 0.15$, a decrease in grain size is observed, while the lattice cell parameter increases and the ratio $I(400)/I(311)$ rises, which is caused by internal changes in the system.

$\varepsilon'/\varepsilon_0$ and $\varepsilon''/\varepsilon_0$ versus temperature in solid solutions of $Li_{1-x}Na_xNi_{0.5}Mn_{1.5}O_4$ are given in Figure 4, $a$ and Figure 4, $b$. The nature of the dependences indicates the absence of a ferroelectric transition in the studied temperature range, which corroborates the version that the disordered spinel $Li_{1-x}Na_xNi_{0.5}Mn_{1.5}O_4$ is not a multiferroic of the II kind. The dependences show that in the temperature range from 15 K to 125 K, the compositions have low values of dielectric constant (below 60). With an increase in the content of $Na^+$, the stability interval $\varepsilon'/\varepsilon_0$ and $\varepsilon''/\varepsilon_0$ is maintained. Above the temperature of 125 K, the dependencies show a sharp increase in the values of $\varepsilon'/\varepsilon_0$ and $\varepsilon''/\varepsilon_0$. Apparently, the main mechanism of electrical conductivity rise in these objects is a hole hopping conductivity between $Mn^{4+}$ and $Mn^{3+}$ cations [28,29].

In the studied system of solid solutions, this mechanism may occur due to the fact that oxygen vacancies are created

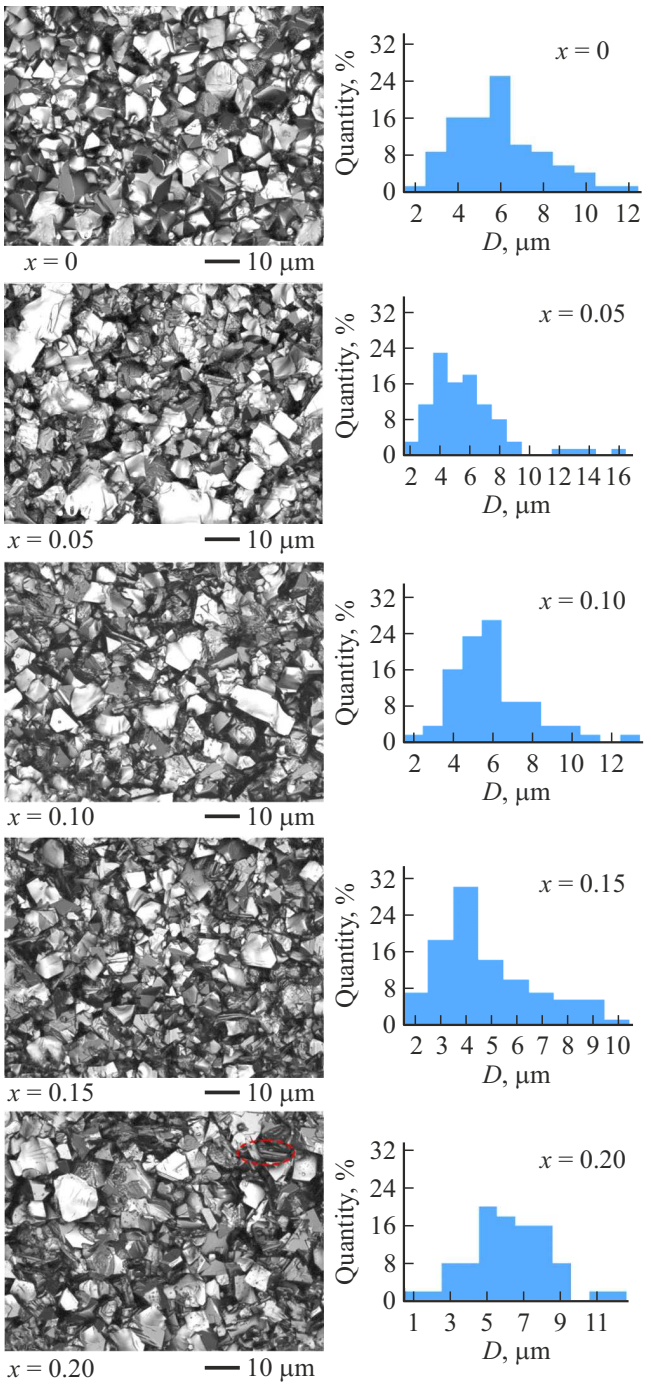


**Figure 3.** Photos of microstructure of the solid solutions of system $Li_{1-x}Na_xNi_{0.5}Mn_{1.5}O_4$.

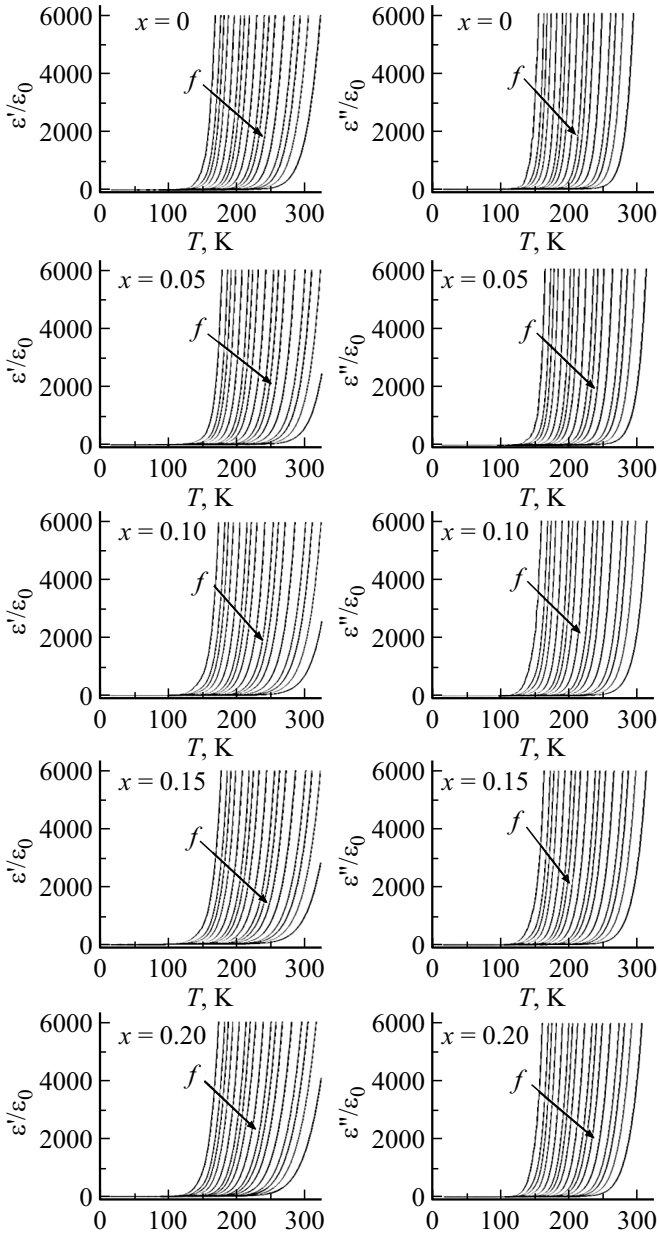


**Figure 4.** Dielectric characteristics $\varepsilon'/\varepsilon_0$ (*a*) and $\varepsilon''/\varepsilon_0$ (*b*) versus temperature within the frequency range of 100 Hz–1 MHz in the solid solutions of the system $Li_{1-x}Na_xNi_{0.5}Mn_{1.5}O_4$.

during high-temperature sintering as a result of electrons release:

$$O \leftrightarrow V^o + 1/2O_2,$$

$$V^o \leftrightarrow V_O^{oo} + 2e'.$$

Higher number of oxygen vacancies can cause a change in the valence state of $Mn^{4+}$. If the released electrons in the system are coupled with $Mn^{4+}$ in the system, the charge Mn $(^{4+\leftrightarrow 3+})$ will be transformed as described below: $Mn^{4+} + e' \leftrightarrow Mn^{3+}$.

## 4. Conclusion

By method of two-stage solid-phase synthesis followed by sintering using conventional ceramic technology, solid solutions were obtained for $Li_{1-x}Na_xNi_{0.5}Mn_{1.5}O_4$ system with $0.00 \le x \le 0.20$, $\Delta x = 0.05$. The solid solutions have a structure of a disordered spinel Fd3m. It is shown that impurity phases of NiO and $LiMnO_2$ are formed in the system, the concentration of which rises with higher concen-

tration of $Na^+$. The X-ray diffraction analysis demonstrated that $Na^+$ cations cannot be integrated into the structure of $LiNi_{0.5}Mn_{1.5}O_4$. In the temperature range from 15 to 125 K, a plateau with values not exceeding 60 K is observed on the dependences $\varepsilon'/\varepsilon_0$ and $\varepsilon''/\varepsilon_0$. The increase in the dielectric constant above 150 K is explained by the hopping conductivity between the cations. $Mn^{3+}$ and $Mn^{4+}$.

### Funding

The study was supported by the Ministry of Science and Higher Education of the Russian Federation (State assignment in the field of research. Project No. FENW-2023-0010/GZ0110/23-11-IF),Equipment was provided by the Center for the Collective Use of Scientific Equipment of the Research Institute of Physics, Southern Federal University, „Electromagnetic, Electromechanical and Thermal Properties of Solid Bodies — Research Institute of Physics, Southern Federal University“.

### Conflict of interest

The authors declare that they have no conflict of interest.

## References

[1] N.A. Spaldin Proceedings of the Royal Society A: Mathematical, Physical and Engineering Sciences **476**, *2233*, 20190542 (2020).
[2] Z.V. Gareeva, E.I. Badertdinova. Izvestiya Ufimskogo nauchnogo tsentra RAN, **44** (2021). (in Russian).
[3] Z. Hu, G.B.G. Stenning, H. Zhang, Y. Shi, V. Koval, W. Hu, Z. Zhou, C. Jia, Is. Abrahams, H. Yan. Journal of Materiomics **11**, 100857 (2025).
[4] J. Cao, B. Yang, G. Smith, A. Mahajan, H. Zhang, Y. Lin, C. Yu, V. Koval. Materials & Design **248**, 113498 (2024).
[5] X. Wang, J. Shi, X. Wang, Y. Li. Ceramics International **46**, *11*, 18707 (2020).
[6] A. Datar, B. Ray, S. Datar, V. Mathe. Journal of Magnetism and Magnetic Materials **489**, 165373 (2019).
[7] J. Finley, L. Liu. Appl. Phys. Lett. **116**, 110501 (2020).
[8] X. Ren, Y. Han, X. Chen, Y. Fu, F. Wang, K. Hu, Z. Sun, K. Zhang. Journal of Alloys and Compounds **920**, 165918 (2022).
[9] Sushanta Mandal, Jyoti Sharma, Tirthankar Chakraborty, Sanjoy Kr. Mahatha, Sourav Marik. Journal of Alloys and Compounds **1010**, 177993 (2025).
[10] A. Sundaresan, N.V. Ter-Oganessian. J. Appl. Phys. **129**, 060901 (2021).
[11] N.W. Grimes Philos. Mag. **26**, 1217 (1972).
[12] J. Hemberger, P. Lunkenheimer, R. Fichtl, H.-A. Krug von Nidda, V. Tsurkan, A. Loidl. Nature **434**, 364 (2005).
[13] A.I. Smolentsev, A.B. Meshalkin, N.V. Podberezskaya, A.B. Kaplun. J. Struct. Chem. **49**, 953 (2008).
[14] Run Liu, Linlin Pan, Silu Peng, Lili Qin, Jian Bi, Jiangtao Wu, Hua Wu, Zuo-Guang Ye. J. Mater. Chem. C. **7**, 1999 (2019).
[15] W. Branford, M.A. Green, D.A. Neumann. Chem. Mater. **14**, 1649 (2002).
[16] R. Santhanam, B. Rambabu. Journal of Power Sources **195**, 5442 (2010).
[17] I. Ganesh. International Materials Reviews **58**, 63 (2013).
[18] G. Liu, L. Wen, Y. Liu. Journal of Solid State Electrochemistry **14**, 2191 (2010).
[19] J. Wang, W. Lin, B. Wu, J. Zhao. Electrochimica Acta. **145**, 245 (2014).
[20] N. Amdouni, K. Zaghib, F. Gendron. Journal of Magnetism and Magnetic Materials. **309**, *1*, 100 (2007).
[21] R. Svetogorov, P. Dorovatovskii, V. Lazarenko. Cryst. Res. Technol, **55**, *5*, 1900184 (2020).
[22] R.D. Svetogorov „Dionis — Diffraction Open Integration Software“. Certificate of state registration of computer program No. 2018660965 (2018).
[23] Powder Diffraction File. Data Card. Inorganic Section. Set 1, card 1239. JCPDS. Swarthmore, Pennsylvania, USA (1948).
[24] Powder Diffraction File. Data Card. Inorganic Section. Set 9, card 109. JCPDS. Swarthmore, Pennsylvania, USA (1948).
[25] G.B. Bokiy. Vvedenie v kristallokhimiyu. Izdatelstvo Moskovskogo universiteta. M. (1954). 120 p. (in Russian).
[26] T. Ohzuku, K. Ariyoshi, S. Takeda, Y. Sakai. Electrochim. Acta. **46**, 2327 (2001).
[27] C. Liu, J. Nan, X. Zuo, X. Xiao, D. Shu. International Journal of Electrochemical Science. **7**, *8*, 7152 (2012).
[28] D.V. Volkov, A.V. Nazarenko, L.A. Shilkina, I.A. Verbenko. Izvestiya RAN. Seriya fizicheskaya, **87**, *9*, 1248 (2023). (in Russian).
[29] T. Li, K. Chang, A.M. Hashem, A.E. Abdel-Ghany, R.S. El-Tawil, H. Wang, H. El-Mounayri, A. Tovar, L. Zhu, C.M. Julien. Electrochem. **2**, 95 (2021).

*Translated by T.Zorina*